Cellular Signalling 62 (2019) 109335

Contents lists available at ScienceDirect

Cellular Signalling

journal homepage: www.elsevier.com/locate/cellsig

New automatic quantification method of immunofluorescence and histochemistry in whole histological sections

Friederike Kessel[a], Anne Steglich[a], Todor Tschongov[a,1], Florian Gembardt[a], Leo Ruhnke[a,2], Julian Stumpf[a], Rayk Behrendt[b], Christian Cohrs[c,d], Irakli Kopaliani[e], Vladimir Todorov[a,3], Michael Gerlach[a,4,3], Christian Hugo[a,*,3]

[a] Experimental Nephrology and Division of Nephrology, Department of Internal Medicine III, University Hospital Carl Gustav Carus at the Technische Universität Dresden, Fetscherstrasse 74, 01307 Dresden, Germany
[b] Institute for Immunology, Carl Gustav Carus Faculty of Medicine, Technische Universität Dresden, Fetscherstrasse 74, 01307 Dresden, Germany
[c] Paul Langerhans Institute Dresden (PLID) of Helmholtz Zentrum München at the University Hospital Carl Gustav Carus at the Technische Universität Dresden, Tatzberg 47, 01307 Dresden, Helmholtz Zentrum München, München-Neuherberg, Germany.
[d] German Center for Diabetes Research (DZD), Ingolstädter Landstrasse 1, 85764 München-Neuherberg, Germany
[e] Department of Physiology, Carl Gustav Carus Faculty of Medicine, Technische Universität Dresden, Fetscherstrasse 74, 01307 Dresden, Germany

ARTICLE INFO

Keywords:
Immunofluorescence
Histochemistry
Automatic quantification
Cell count
Morphology

ABSTRACT

Immunofluorescent staining is a widespread tool in basic science to understand organ morphology and (patho-) physiology. The analysis of imaging data is often performed manually, limiting throughput and introducing human bias. Quantitative analysis is particularly challenging for organs with complex structure such as the kidney. In this study we present an approach for automatic quantification of fluorescent markers and histochemical stainings in whole organ sections using open source software. We validate our novel method in multiple typical challenges of basic kidney research and demonstrate its general relevance and applicability to other complex solid organs for a variety of different markers and stainings. Our newly developed software tool "AQUISTO", applied as a standard in primary data analysis, facilitates efficient large scale evaluation of cellular populations in various types of histological samples. Thereby it contributes to the characterization and understanding of (patho-) physiological processes.

1. Introduction

Detailed understanding of cellular composition and organ architecture is a prerequisite to examine and understand physiological and pathological processes in humans and experimental animals. Multiple experimental techniques are commonly utilized to assess tissue composition in experimental models, including fluorescence activated cell sorting (FACS) and a variety of histological techniques. Especially in

Abbreviations: FACS, fluorescence activated cell sorting; CTI, cortical tubulointerstitum; DAPI, 4′,6-diamidino-2-phenylindole; RGB, Red/Green/Blue; ROI, Region of interest; AT2, angiotensin II; Gsα, stimulatory G protein α-subunit; PCNA, proliferating cells nuclear antigen; TUNEL, terminal deoxynucleotidyl transferase-mediated dUTP-biotin nick end labeling; dUTP, deoxyuridine triphosphate; TGF-β, transforming growth factor β; PAS, Periodic acid - Schiff; PFA, paraformaldehyde

* Corresponding author at: Department of Internal Medicine III, Division of Nephrology, University Hospital Carl Gustav Carus at the Technische Universität Dresden, Fetscherstrasse 74, 01307 Dresden, Germany.
E-mail addresses: Friederike.Kessel@uniklinikum-dresden.de (F. Kessel), Anne.Steglich2@uniklinikum-dresden.de (A. Steglich), tschoto@outlook.de (T. Tschongov), Florian.Gembardt@uniklinikum-dresden.de (F. Gembardt), Leo.Ruhnke@uniklinikum-dresden.de (L. Ruhnke), Julian.Stumpf@uniklinikum-dresden.de (J. Stumpf), rayk.behrendt@tu-dresden.de (R. Behrendt), Christian.Cohrs@tu-dresden.de (C. Cohrs), irakli.kopaliani@tu-dresden.de (I. Kopaliani), Vladimir.Todorov@uniklinikum-dresden.de (V. Todorov), Michael.Gerlach@uniklinikum-dresden.de (M. Gerlach), Christian.Hugo@uniklinikum-dresden.de (C. Hugo).
[1] Currently University Medical Center Freiburg, Center for Pediatrics and Adolescent Medicine, Hugstetter Straße 55, 79,106 Freiburg, Germany.
[2] Currently Center for Hematology and Blood Stem Cell Transplantation, Department of Internal Medicine I, University Hospital Carl Gustav Carus at the Technische Universität Dresden, Fetscherstrasse 74, 01307 Dresden, Germany.
[3] Equal contributions.
[4] Currently Core Facility Cellular Imaging (CFCI), Carl Gustav Carus Faculty of Medicine, Technische Universität Dresden, Fetscherstrasse 74, 01307 Dresden, Germany

https://doi.org/10.1016/j.cellsig.2019.05.020
Received 24 April 2019; Received in revised form 31 May 2019; Accepted 31 May 2019
Available online 03 June 2019
0898-6568/

complex fields of research, involving various cellular markers and cell types as well as extracellular matrix the utilization of one single approach for evaluation and quantification is limited.

While FACS is able to analyze multiple cellular markers for high cell numbers, it typically requires large sample sizes and disintegration of solid tissue. On the other hand classic histochemistry preserves tissue integrity but is more restricted in marker multiplexing. In addition, non-homogeneous, asymmetric tissue architecture leads to various challenges for quantitative structural examination of solid organs. Immunofluorescent staining circumvents marker-related restrictions by the use of multiple specific antibody-based probes. Recent advances in microscopy have enabled the collection of vast amounts of high-resolution ultrastructural data in a standardized and reproducible way without researcher intervention. To quantify these images in the context of a specific scientific question, the researcher aims to extract numerical data by reducing the original data complexity in an image analysis process [1]. The straightforward and frequently performed approaches are manual counting and often imprecise semi-quantitative indexing. These methods are simple but also prone to different forms of bias and ultimately limited by human workload.

Computational analysis has the potential to overcome these restrictions [2] by extracting more detailed data from image files using fixed algorithms for image processing and segmentation. An automatic approach can largely eliminate human bias and workload and thus utilize the full potential of modern imaging methods. The open source software FIJI [3] allows researchers to perform batch image analysis and automatize measurements. Marker-specific image processing algorithms are applied to separate marker positive areas from background and noise and thereby segment the original image data. A central aspect of these processes is the determination of the threshold value separating actual signal from background. Multiple strategies have been described [4], including fixed and adaptive thresholds which can be determined locally or over the whole image. Due to the variability in marker characteristics (localization and intensity) the utilized thresholding strategy has to be adapted to obtain bona fide results.

Automatic analysis is able to produce vast amounts of complex numerical data [2], which needs to be abstracted and reduced to address specific questions. To handle multiple ten thousand entities the statistic computing software R [5] and associated packages provide all the necessary tools.

In the present study, we combined automatic microscopy with an automatic FIJI-based analysis workflow for reliable quantification of populations of marker positive cells or marker positive area in whole histological sections. We demonstrate the versatility of the analysis to different markers (cytoplasmatic and nuclear markers, extracellular matrix) and stainings (immunofluorescence and histochemistry). These analyses were performed in different organs (heart, kidney, pancreas, skin) with the help of various animal models (Angiotensin II (AT2) mediated cardiac remodeling, inducible Gsα knockout in renin cells, serum mediated kidney injury, streptozotocin (STZ) induced diabetes and skin cancer, see also Suppl. Table 1). Using R we established and exploited a database structure incorporating results from automatic image processing. We aimed to maximize sensitivity for the quantification of even rare events in different types of stainings and minimize researcher interaction and workload while maintaining full reproducibility.

2. Materials and methods

2.1. Animal experiments

All animal experiments were conducted in accordance with the EU Directive 2010/63/EU for animal experiments, institutional guidelines and state laws of Saxony and were approved by the Landesdirektion Sachsen under the registrations DD24-9168.11-1/2012-45, DD24-5131/338/56, DD24-5131/338/23 and DD24-5131/338/65. Mice were housed in standard cages with a maximum capacity of 5 animals at a 12/12 light/dark cycle. If not stated otherwise, mice had ad libitum access to standard chow and water.

2.1.1. AT2-treatment

Cardiac remodeling in wild type mice (BL6JoLaH, Harlan) was induced with 4-weeks infusion of 1.5 mg/kg/day angiotensin II diluted in 0.9% NaCl. Angiotensin II was infused using osmotic minipumps (Alzet® model 2004) implanted subcutaneously under anesthesia with 2% Isoflurane. Control mice were infused with 0.9% NaCl. Osmotic minipumps were implanted at the age of 12 weeks. Mice were sacrificed with 90 mg/kg Ketamine/10 mg/kg Xylazine solution.

2.1.2. Inducible Gsα knockout

We generated the renin-reporter mouse strain mRen-rtTAm2-LC1-tdT mice by crossing our inducible renin-producing cell strain mRen-rtTAm2-LC1 [6] with commercially available red fluorescent protein (tdTomato; tdT) expressing strain B6.Cg-Gt(ROSA)26Sortm9(CAG-tdTomato)Hze/J [Jackson Laboratory, Stock No. 007914]. These mice were further crossed with our Gsα-floxed mice [7]. 6–8 weeks old male and female quadruple transgenic mRen-rtTAm2-LC1-tdT-Gsα fl/fl (C57BL/6 J) mice and Gsα wt/wt littermates received drinking water, supplemented with 2 mg/ml doxycycline, 10 mg/kg bodyweight enalapril and 5% sucrose ad libitum for 18 days. This pulse-induction was followed by a continuous doxycycline induction for up to 3 months by ad libitum chow (R/M-H, +625 mg/kg doxycycline; ssniff Spezialdiäten GmbH, GER). 1 month after beginning of food induction, unilateral nephrectomy (UNx) was performed. Animals were sacrificed after 3 months of food induction and the remaining kidney was harvested (Suppl. Fig. 1).

2.1.3. Serum mediated kidney injury

8–12 weeks old male C57BL/6J mice were treated with test sera raised against mouse kidney cells as previously reported [6]. Animals underwent UNx after 2 days and were sacrificed on day 6 and kidneys were harvested (Suppl. Fig. 2).

2.1.4. STZ-induced diabetes

8 weeks old male C57BL/6J mice received an i.p. injection of 180 mg streptozotocin/kg bodyweight in 50 mM sodium-citrate buffer pH 4.5 after not having access to food for 6–8 h. Control animals received equivalent injection of buffer. After injection the mice received water with 10% sucrose. 16 weeks after injection mice were sacrificed and kidneys harvested.

2.1.5. Pancreas

A 12 week old C57BL/6J mouse was sacrificed and the pancreas was harvested, fixed in 4% paraformaldehyde (PFA) for 2 h, submerged in a sucrose gradient and embedded and frozen in Tissue-Tek (Sakura). Sectioning was performed with a cryostat at 10 µm section thickness.

2.1.6. Mouse skin cancer model

Mice deficient for DNA repair (Epidermis-specific knockout of RNaseh2b: *Rnaseh2b$^{fl/fl}$-K14Cre*) and irradiation protocols were described previously [17].

2.2. FACS analysis

Sample preparation and gating protocols for FACS analysis were performed as previously reported (Suppl. Fig. 3) [8,9]. In brief, kidneys were digested with collagenase 1A and DNase 1, the suspension was filtered, quantified for cell number, fixed, permeabilized and a directly labeled renin antibody. The antibody was labeled using the Alexa Fluor 647 Monoclonal Antibody Labeling Kit (Thermo Fisher) according to the manufacturer's instructions.

2.3. Sampling, sectioning and staining for fluorescent microscopy

For 2 µm thick paraffin sections, kidneys were fixed in freshly prepared 4% PFA or zinc-fixative (0.05% calcium acetate, 0.5% zinc acetate, 0.5% zinc chloride *w/v* in 0.1 M TRIS buffer, pH 7.4) at 4 °C overnight. Kidneys were dehydrated and embedded in paraffin. For the preparation of 6 µm thick cryosections, kidneys were fixed in freshly prepared 4% PFA at 4 °C overnight and incubated in 18% sucrose at 4 °C overnight. Subsequently, the kidneys were embedded in Richard-Ellen Scientific NEG-50™ (Thermo Fisher Scientific) and frozen on dry ice prior to cryotome cutting. Immunofluorescent staining was performed after acetone fixation (cryosections) or rehydration (paraffin sections). For α-8-integrin and PCNA staining samples underwent an antigen retrieval by cooking sections in 10 mM sodium-citrate buffer for 3 min. Permeabilization with 0.5% Triton-X100 in tris-buffered saline (TBS) for 20 min at room temperature (RT) was done for PCNA and renin staining. Samples were blocked in 5% serum (goat/donkey) in 1% bovine serum albumin (BSA) in TBS for 30 min at RT prior to incubation with primary antibody over night at 4 °C. Secondary antibody was incubated for 2 h at RT. All samples were counterstained with DAPI before mounting with mowiol mounting medium (Sigma Aldrich, Germany). The complete list of antibodies used in this study is provided in Suppl. Table 2. TUNEL staining with Click-iT Plus TUNEL Assay was performed according to the supplier's protocol, with exception of nuclear counterstaining with DAPI instead of Hoechst33342. To assess fibrosis, 5 µM paraffin sections of PFA-fixed hearts were stained with Fast green/Sirius red staining for collagen I and III as previously described [10]. Briefly, sections were deparaffinized with xylene and rehydrated with ethanol. After 1 h staining in 1% Fast green/Sirius red (Sigma) solution sections were washed in H_2O, dehydrated with ethanol and xylene and embedded using DePeX (Serva, Heidelberg, Germany). Skin and pancreas stainings were performed as previously described [11,12].

2.4. Automatic microscopy

Automatic microscopy was performed on an upright stand Zeiss Axio Scan of the Light Microscopy Facility, a Core Facility of the CMCB Technology Platform at TU Dresden with the following filters: DAPI Ex 365, BS 395, Em 445/50; eGFP Ex 470/40, BS 495, Em 525/50; Cy 3 Ex 550/25, BS 570, Em 605/70; mPlum Ex 587/25, BS 605, Em 647/70 using Zeiss Plan-Apochromat 20 × 0.8 NA Objective and Zeiss Plan-Apochromat 40 × 0.95NA corr. Objective. *Z*-Stack was recorded and definite focus was applied. For immunofluorescent stainings the acquisition of digital images of whole mouse kidney sections with a pixel size of 0.325 µm resulted in 16-bit images of about 400 megapixel each. Lateral pixel size corresponded to 0.325 µm (20× objective) and 0.1625 µm (40× objective) respectively. 4′,6-diamidino-2-phenylindole (DAPI) stained nuclei and immunofluorescence stained cellular markers ("co-marker channels") were resolved uniformly over the entire sections (Fig. 1B). Brightfield images were recorded with a lateral pixel size of 0.211 µm with an RGB-camera with uniform white balance.

2.5. Main program

Image and data analysis algorithms were programmed in FIJI (https://fiji.sc/) and R (Version 3.4.3, https://cran.r-project.org/bin/windows/base/old/3.4.3/) and run as a full program in R under RStudio [13] (https://www.rstudio.com/). For FIJI, following plugins were used: MorphoLibJ (https://imagej.net/MorphoLibJ), Adaptive threshold (https://sites.google.com/site/qingzongtseng/adaptivethreshold). In R, following packages and their dependencies are necessary: ggplot2 [14] and reshape2 [15].

All data presented in this study could be processed and analyzed with an Intel® Core™ i5-CPU 3.2GHz processor with Windows 7 as an operating system and 15.8 GB available RAM. Depending on the size of the raw files these requirements may differ.

The source code and basic folder structure for the FIJI macros and R programs necessary to process Axio Scan acquired .czi-files as described for analysis of whole murine kidney sections is available on GitHub (https://github.com/NephrologieDresden/AQUISTO). Sample data will be provided upon reasonable request.

The program "AQUISTO.R" can be opened in RStudio and run from source after setting the paths for the execution file for FIJI ("dirfiji") and the location main directory for the files ("dirdata"). After choosing a task, the program automatically starts data and file processing, runs FIJI macros from the command line or opens Excel tables for user input if necessary. For more information, please refer to the program manual. A graphic summary of the program algorithm description is included in the supplement (Suppl. Fig. 4).

2.5.1. Preparation

The preparation steps are used to prepare raw .czi-files acquired by the Zeiss Axio Scan for actual processing and analysis in a user friendly and computer assisted way. These .czi-files contains images for every section on a slide. In the first step a size reduced preview image (1:16) is generated for every section and saved together with the information about the location on the slide (macro image) and the slide label ("Preparation" > "Get slide headers and previews", ImageJ-Macro "Header_SplitScenes_Previews.ijm"). With this information a database about all available sections is generated, assigning every section on every slide to an identifier and its corresponding staining. There is also the possibility to mark damaged sections or scanning errors in this table with the help of the previews, preventing the images to be used for further evaluation. This is not only useful to record all available samples, but also necessary for the automatic renaming and sorting of these files ("Preparation" > "Add file names to list", ImageJ-Macro "Entering_File_Names.ijm"). In an additional step further input about every staining is entered. This includes information about the scanned co-marker channels, the name of the sectioned organ and tissue compartments that should be selected. Minor tissues refer to small tissue compartments that cannot be selected in an overview picture of the section (like glomeruli in the kidney or islets in the pancreas) ("Preparation" > "Add general information about a new staining", included in the main R-Script). According to this information the previews created in the first step are automatically renamed, relocated to the folder "Experiments" and assigned to a lab member, experiment and staining. Additional folders applying to every staining, like folders for results, images and the analysis are created. Furthermore subfolders indicating the tissue compartments and order of the co-marker channels are generated. Depending on the necessity to select minor tissues and crop these details from the original image the folders "Tiles" and "Cropped_*" are set up ("Preparation" > "Sort and rename files", R-Script "Sample_Characterization.ijm").

2.5.2. Preprocessing and manual selections

In the next manual step the size reduced preview is opened and the section area is recognized automatically. Artifacts can be removed from the region of interest (ROI) and the additional tissue compartments can be selected according to the information given in previous steps ("Manual selection" > " Major tissue selection", ImageJ-Macro "Tissue_Selection.ijm"). If the selection of a minor tissue compartment is necessary parameters have to be set for the creation of the tiles with the assistance of another macro for fluorescent stainings. After selecting a, for the minor tissue representative, area in the preview image, an array for every channel is created showing the output with different parameters for lookup tables (LUT), brightness and contrast. The channel number, maximum value, LUT and number of columns and rows the image should be split into for optimal selection of the minor tissue compartment can be entered ("Preprocessing" > "Set parameters for tiles", ImageJ-Macro "Tile_Parameters.ijm"). In the next step the full sized image is opened from the raw .czi-files and cropped to the previously selected tissue area. For fluorescent stainings every channel is saved as a separate image file in a folder with the identifier name assigned to this section. Brightfield images are converted to RGB-colour images At the same time pixel intensity distributions are saved for every channel and section

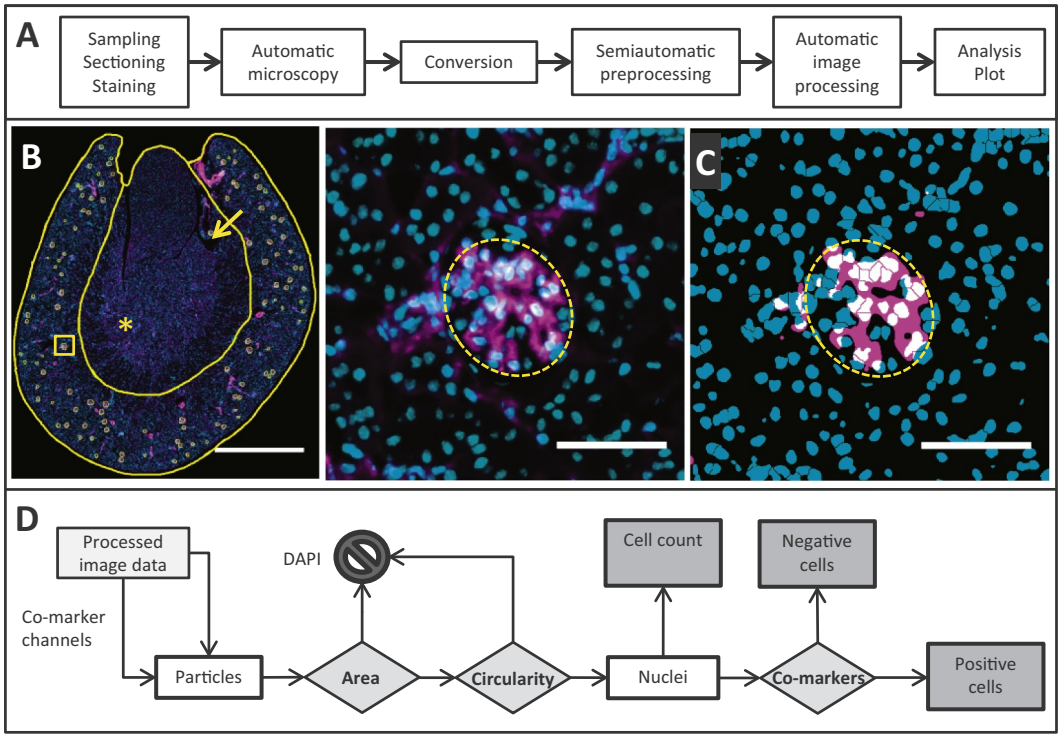

Fig. 1. Workflow for automatic cell based quantification of immunofluorescent stainings in mouse kidney.
A, General scheme of our "AQUISTO" workflow. **B,** Left panel: Whole mouse kidney section stained for mesangial cell marker α-8-integrin (magenta), nuclei stained with DAPI (cyan). Scale bar corresponds to 1000 µm. Semiautomatic morphological preprocessing results in selection of medulla (asterisk), glomeruli (example boxed) and cortical tubulointerstitium (CTI, arrow). Right panel: Actual image resolution at the position indicated by the yellow box in the left panel.. Scale bar: 50 µm. Yellow dashed line in B and C indicates glomerlular tuft. **C,** Corresponding segmented image with automatically detected particles (cyan), α-8-integrin positive area (magenta) and overlap between nuclei and α-8-integrin (white). Scale bar: 50 µm. **D,** Scheme for automatic classification of detected particles in raw database. Parametric exclusion by area and circularity of particles results in nuclei database. Subsequent parametric classification by co-marker channel positivity leads to categorization of nuclei. (For interpretation of the references to colour in this figure legend, the reader is referred to the web version of this article.)

and, if applicable, the image is split to tiles, which are processed as set in the previous step ("Preprocessing" > "Create Images/Tiles", ImageJ-Macro "Images.ijm"). In these tiles the minor tissues can now be selected manually. Upon start of this program part the tiles for one biopsy are opened as a virtual stack. After selection of the ROI it can be added to the ROI-Manager by pressing "t". Confirming the selection after going through the entire stack closes the stack and opens the next one ("Manual Selection" > "Minor tissue selection", ImageJ-Macro "Tile_tissue_Selection.ijm"). The ROIs for the tissue compartments and minor tissues are automatically recalculated to fit the full size image. The minor tissues are also combined to one selection and added to the major tissue compartments as one ROI. After the selections for the minor tissue compartments are complete it is possible to crop these areas as details from the full size image ("Crop minor tissues", ImageJ-Macro "Crop_minor_tissues.ijm").

2.5.3. Setting parameters

Before the actual processing, parameters have to be set for every channel. For this 2000 × 2000 pixel big details from the original images are selected. To make sure these samples cover the range of differences in staining intensity through the staining set there is a histogram analysis for the pixel intensity distributions generated for every channel during image creation ("Fluorescence Processing"/"Brightfield Processing" > "Histogram Analysis", R-Script "Histogram_Analysis.ijm"). When choosing the sections for the parameter setting 5 to 10 samples, showing high differences in pixel intensity distribution in these histograms, should be selected. After the selection of representative areas in these images in the previews, the full sized image is opened in the background, the details are cropped according to the information and saved as single channel images ("Fluorescence Processing"/"Brightfield Processing" > "Choose samples", ImageJ-Macro "Sample_Selection.ijm"). When setting the parameters for nuclei an array can be created with the DAPI channel of the first of these details. It contains different parameter combinations altering the threshold for DAPI positive area, the radius of the Gaussian blur prior to maximum detection and the noise tolerance for maximum detection. The chosen parameters are then tested in every sample detail previously saved. This can be repeated until the results represent the optimal recognition of DAPI particles for every sample ("Fluorescence Processing" > "Parameter setting nuclei", ImageJ-Macro "Watershed_Array.ijm"). Setting the parameters for co-marker segmentation works in a similar way. The co-marker segmentation is divided into three main steps: The first step includes background adaption, either through a linear shift of the histogram to set background intensity to the baseline or by background subtraction with a FIJI plugin, and filters to equalize staining intensity and reduce noise. For segmentation a fixed threshold or a threshold adapted to median pixel intensity and intensity standard deviation can be set. Postprocessing steps include the dilation of the signal and exclusion of dark and bright particles. If necessary an array showing different combinations of filters, background adaption and fixed or adaptive thresholds is generated for the corresponding co-channel of the first detail image. After visually deciding for a set of functioning parameter combinations they can equally be tested for all image details of the co-channel until a parameter combination is found that segments all image details correctly ("Fluorescence Processing"/"Brightfield Processing" > "Parameter setting co-channel", ImageJ-Macro "Channel_Array.ijm"). Information about the chosen parameters for DAPI and co-channel segmentation are saved as a text file (*\Macros\Processing).

2.5.4. Processing

Once the corresponding parameters are set, the sections can be processed channel by channel. For the detection of nuclei the marker-controlled watershed is performed and the detected particles are saved

as a single ROI for every image ("Fluorescence Processing" > "Channel Processing", ImageJ-Macro "Nucleus_Detection.ijm"). For the co-channels, after applying filters and background adaption, the image is duplicated and only one copy is segmented. The ROI-Set for the tissue selection and tissue compartments is loaded and overall positive area is measured for every tissue compartment in the segmented image. The mean pixel intensity in the unsegmented image is measured in a similar way. Subsequently – in fluorescent images - the ROI for the detected particles in the DAPI channel is loaded and used to create a black and white image with segmented particles. Every single particle is analyzed for the different tissue compartments for overlap with the segmented co-channel image and mean pixel intensity in the unsegmented co-channel image. If minor tissue compartments where selected every single entity is measured separately in the same way as described for tissue compartments (total co-marker positive area, mean intensity, co-marker overlapping with every nucleus and intensity in every nucleus). Additionally for every particle area and circularity is assessed ("Fluorescence Processing"/"Brightfield Processing" > "Channel Processing", ImageJ-Macro "Channel_Detection.ijm").

2.5.5. Database analysis

To make the database more accessible for users and give an overview about possibly interesting changes between groups and tissue compartments we used statistical computing with R. For the results from every section to be grouped in a reasonable way the algorithm requires the table "*\Analysis\Groups.csv" to be filled out, assigning every section to an experimental group. The order of experimental groups can be set as well after starting this program step. For the co-marker positive area and co-marker intensity in the tissue compartments a summary table is generated, combining the results from all co-markers. This is repeated for the minor tissue compartment, with a separate table for every co-marker and selection area and statistical values like mean, standard deviation, minimum and maximum for every section. The combined lists for every single entity within a section are available in a subfolder. To analyze the contents of the DAPI particle database particles are defined as valid nuclei by parametric exclusion. For this distribution histograms of particle area and circularity are generated and limits can be set. For nuclei in a mouse kidney section an area between 6 and 45 μm^2 and a circularity of > 0.5 were reliable predictors for correct detection of valid nuclei. In the next step nuclei are classified as co-marker positive by co-marker overlap or intensity. To set these thresholds, the staining intensity, intracellular co-marker localization and processing strategies, especially postprocessing steps like signal dilation are important. Distribution histograms about co-marker coverage distributions are set up to support this decision. With these parameters, a data table listing the indices of every excluded particle and of particles positive for each co-marker is created. This file contains very long arrays of numbers assigning single particles to their classification as correct nuclei and co-marker positivity. With this information the fraction of co-marker positive nuclei can be calculated, but the data table can also serve as the source for backtracing events in the original image. Summary tables listing the total number of nuclei and co-marker positive nuclei in every tissue compartment are created. For minor tissue compartments additional tables with statistical information about standard deviation and tables listing numbers of nuclei and fraction of co-marker positive nuclei for every single entity are made. Through combination of the total area of a tissue compartment and the number of nuclei within, the nuclear density can be calculated. Overview graphs are automatically generated to visualize the results summarized in the data tables, while grouping the results to different tissue compartments and experimental groups ("Analysis" > "Standard Analysis", R Script "Slidescan_Analysis.R").

2.6. Statistics

To assess significant changes between multiple groups *p*-values were calculated with a pairwise *t*-test in R without adjustments for p-values. Differences were considered to be significant if $p < .05$ (marked with an asterisk in the corresponding figures). Correlation was calculated with Pearson's correlation coefficient in R.

3. Results

3.1. Establishment of a workflow to automatically acquire and analyze whole mouse organ sections

Although the workflow presented in this study can be applied to different organs it was primarily developed for the analysis of kidney tissue. Due to its morphologic complexity, the kidney is a representative example for many problematic issues in image analysis. It is comprised of functional units called nephrons. Nephrons consist of glomeruli and tubuli, each containing various cell types with highly specialized functions. To minimize human bias and workload in image analysis of this complex morphology, we developed a novel workflow combining automatic microscopy with automatic processing of digital image files and automatic data analysis (Fig. 1A). This enabled consistent image processing in complete experimental sets utilizing the open source programs FIJI [3] and R [5].

For sampling, sectioning and staining conventional protocols were applied and sections were scanned with a Zeiss Axio Scan Z1, resulting in uniform, automatically acquired high-resolution images of intact sections. We created a data infrastructure defining a stringent workflow (Suppl. Fig. 5) for all image data files including data conversion, renaming and assignment to the appropriate folder. A computer assistedpreprocessing step was performed to spatially select medulla, glomeruli and remaining cortex (cortical tubulointerstitium, CTI) of kidney sections by morphology (Fig. 1B), allowing for distinct analysis of these tissue compartments. Preprocessing was optimized by the creation of size-reduced preview images and the use of a graphics tablet. During the selection the section is recognized automatically and additional tissue compartments can then be selected within the batch process for all samples. Plotting of pixel intensity distributions for all sections included in an experimental set supported detection of variations in staining intensity and marker positivity for each channel (Suppl. Fig. 6).

The base macro could be individually customized for any organ, tissue compartment and type of staining, for optimal segmentation of all co-markers. Processing parameters for nucleus detection (only for immunofluorescent stainings) and co-marker segmentation were set and verified in representative 2000 × 2000 pixel details of 5 to 10 images for every staining set. These regularly included staining controls and sections that covered the entire range of staining intensities, visualized in the intensity histogram distributions.

For immunofluorescent stainings, images were batch-processed in FIJI resulting in binary images of 4′,6-diamidino-2-phenylindole (DAPI) and co-marker channels (Fig. 1C). We based the quantification of cells on the automatic detection of particles in the DAPI channel by the plugin "MorpholibJ marker-controlled watershed" [16]. A database of all recognized DAPI particles in a kidney section was created. It included size, shape and spatial parameters as well as values for overlap with positive co-marker signal and co-marker intensities for each detected particle, co-marker channel and tissue compartment (Fig. 1D). The overall marker-positive area was recorded as well. For histochemical stainings, the Red/Green/Blue (RGB) images were unmixed with settings applying to the respective type of staining using the plugin "Colour Deconvolution" [17] and segmented, resulting in a binary image of the marker-positive area, which was then measured.

To reduce data complexity and analyze the contents of the database, we subsequently performed statistical computing with R. Histogram distribution analysis of particle size, circularity, co-marker coverage and co-marker intensity was performed to manually set thresholds defining nuclear identity and co-marker positivity for immunofluorescent stainings. The total number of detected nuclei and the fraction of co-

marker positive nuclei were summarized in data tables for each experiment. More over the marker-positive area fraction in every tissue compartment was assessed Furthermore, other morphologically relevant variables like tissue area and total numbers of nuclei were registered. These tables were the main resource for further data evaluation.

All relevant data necessary for complete reproducibility (original images, semiautomatic selections, detected regions of interest (ROI) sets and image processing macros) were stored (Suppl. Fig. 5).

3.2. Reliability of automated identification and classification of nuclei

In our approach nuclear detection in fluorescent sections relied on the separation of DAPI stained particles by the plugin "MorpholibJ marker-controlled watershed" [16]. In brief, in the DAPI channel (Fig. 2A) the DAPI positive area was defined, edges to background were created and maxima were detected within the image (Fig. 2B). From every maximum located in a DAPI positive area the surrounding pixels were flooded until reaching an edge or a different flooded area, which was then separated. This resulted in binary images with separated particles (Fig. 2C). For optimal nuclear detection three parameters were adapted: To ensure only finding one maximum per nucleus the image was processed with a Gaussian filter to equalize granules (Fig. 2D) and the noise tolerance for maximum detection was set (Fig. 2E). For the recognition of DAPI positive area and its edges the intensity threshold was defined (Fig. 2F). With these parameters the DAPI channel of every section in a staining set was processed equally. Detected particles were saved as a ROI set for the section.

During image analysis size and shape parameters are registered for every DAPI particle to further verify nuclear identity of the recognized particles. Since nucleus recognition via DAPI signal is the key step of our approach, we verified our parametric exclusion for nucleus detection by manual review of the automatic particle analysis (Fig. 2G). Multiple randomly selected areas of kidney sections with a total sum of 5370 nuclei were assessed. In a manual classification, 13% of automatically detected particles were rejected, being mostly incompletely separated nuclei or very small DAPI particles. From the comparison of verified and rejected particles we identified area and circularity as reasonable predictors for nuclear identity in the kidney. Major discrepancies between verified and rejected nuclei were found within the categories $< 6\,\mu m^2$ and $> 45\,\mu m^2$ of area and < 0.5 of circularity. Subsequently, we applied these thresholds to minimize false detection of nuclei. 91% of valid nuclei are located within this "gate", representing the "yield" of the method. 26% of the invalid particles were also included in the analysis, resulting in an overall error rate of 3.3%.

3.3. Segmentation strategies for co-marker channels

Strategies to segment positive signal from background in the co-marker channels rely largely on signal intensity (Fig. 3A–B) and intracellular localization of the marker. For the stainings presented in this study, but also for all markers stained and tested for analysis with "AQUISTO" in our research group, we found a small set of commands in FIJI sufficient. To unmix RGB images of histochemical stainings into separate channels, different methods of colour deconvolution can be applied. During this process a brightfield image is split into 8-bit channels based on the stain-specific RGB absorption [17], resulting in the possibility to segment and process the channel analogous to fluorescent images.

A Gaussian or median filter reduces noise within marker positive areas and equalizes staining intensity. Background subtraction [18] may significantly enhance the signal to noise ratio but can also enhance the intensity of staining artifacts. A general histogram adaption, setting the background pixel intensity to the baseline, also increases signal to background ratio while only having a linear impact on the general intensity distribution (Fig. 3C). For segmentation a fixed value can be applied (Fig. 3D–E) if staining quality is very consistent over the entire set. We also found that applying a threshold adapted to median pixel intensity and intensity standard deviation provides good results (Fig. 3F–G). However, this method is restricted to stainings with < 50% of co-marker positive area and a limited variance of co-marker positivity between the sections. Once the co-marker channel is segmented to a binary image post-processing steps can enhance nuclear coverage (dilation of the signal in immunofluorescent stainings), especially for cytoplasmatic markers, or exclude small artifacts (removal of small bright and dark outliers). All processing parameters used for the quantification of stainings mentioned in this study are listed in Suppl. Table 3.

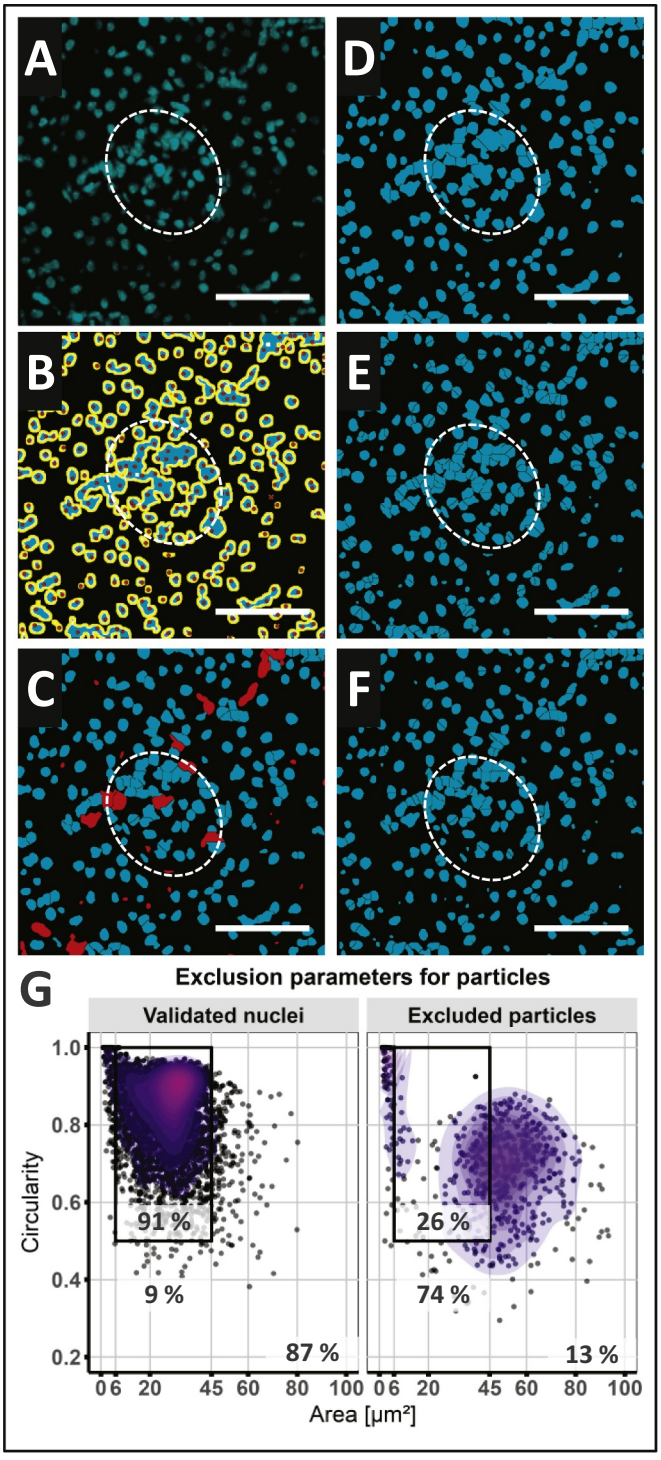

(caption on next page)

Fig. 2. Verification of nuclear detection.
A-F, DAPI stained nuclei (cyan) of image detail from Fig. 1C (A). Scale bar: 50 µm, glomerular area is indicated by white circle. Particles were detected with the plugin "MorpholibJ marker-controlled watershed" [16] using three morphological anchors (B): DAPI-stained areas (cyan), edges (yellow) and signal maxima (red). Separated particles in the processed image (C) are classified as valid nuclei or excluded particles (red) by parametric exclusion according to particle size and circularity. Parameters in nucleus detection (D-F): Increasing the sigma of the Gaussian blur prior to maximum detection leads to a lower number of detected maxima (D). Decreasing the noise tolerance during maximum detection results in detection of more maxima (E). Decreasing the lower threshold leads to smaller areas and a higher tendency to split entities (F). **G,** Exclusion parameters for classification of DAPI particles by manual validation. Left panel: Automatically detected DAPI particles verified as nuclei; right panel: automatically detected DAPI particles rejected by manual verification. Black boxes indicate chosen classification parameters for nuclei in the kidney. (For interpretation of the references to colour in this figure legend, the reader is referred to the web version of this article.)

3.4. Consistency in consecutive sections and backtracing of events

To ensure the consistency of our processing over multiple samples, we analyzed a set of 21 consecutive kidney sections stained for α-8-integrin, a mesangial cell marker, from a healthy mouse. We quantified the fraction of α-8-integrin positive nuclei in the glomeruli with a fixed threshold and increased nuclear coverage of the cytoplasmic staining by dilation of the signal. Nuclei that overlapped > 95% with the α-8-integrin signal were considered to be positive. We could robustly detect 28% ± 1.8% α-8-integrin positive cells inside glomeruli (Fig. 4A), which is in line with prior reports [19]. Single glomeruli within serial sections showed a high variance of α-8-integrin positivity (mean intrasample standard deviation 14.0%), reflecting the typical pattern of 2-dimensional analysis of complex 3-dimensional anatomical structures [20]. This indicates that the intersample standard deviation is 7.8 times lower than the intrasample standard deviation, demonstrating a high consistency of consecutive sections. To be able to visually verify our results, we used the inherent characteristic of a database approach to identify entities in an analyzed dataset and automatically visualize them in the original image data. For example glomeruli with an unexpectedly low or high fraction of α-8-integrin can be traced back in the original image (Fig. 4B). Since every single nucleus is recorded with its marker positivity, area, circularity and position it can be retraced in the original image to directly visualize the results (Fig. 4C).

The analysis of 21 kidney sections included a total number of 2.2 million nuclei and consumed 8 h work time, requiring 3 h of active researcher interaction (semiautomatic preprocessing and processing parameter adjustment) and 5 h of computing time. This corresponds to roughly 12,000 counts per minute within the manual steps. Even with the optimistic assumption of 150 manual counts per minute, this equals the workload of > 80 persons in the same time frame.

3.5. Quantification of extracellular matrix in brightfield images

In contrast to the quantification of cell numbers in immunofluorescent sections (α-8-integrin positive cells in the kidney) we next used the same workflow to assess the marker-positive area in histochemically stained sections. These sections were obtained from the hearts of mice which were infused with either AT2 treatment and their respective NaCl controls (Fig. 5A). We could reliably measure the marker positive area in the Fast green/Sirius red stained section after colour deconvolution for Giemsa staining and segmentation with a fixed threshold over the entire staining set of 22 sections. After AT2 infusion the sections display a significant increase in overall tissue area ($p < .001$, *t*-test) and the fraction of marker positive area ($p = .015$, *t*-test) when compared to controls (Fig. 5B). These effects underline the general pro-fibrotic nature of the applied mouse model [21], resulting

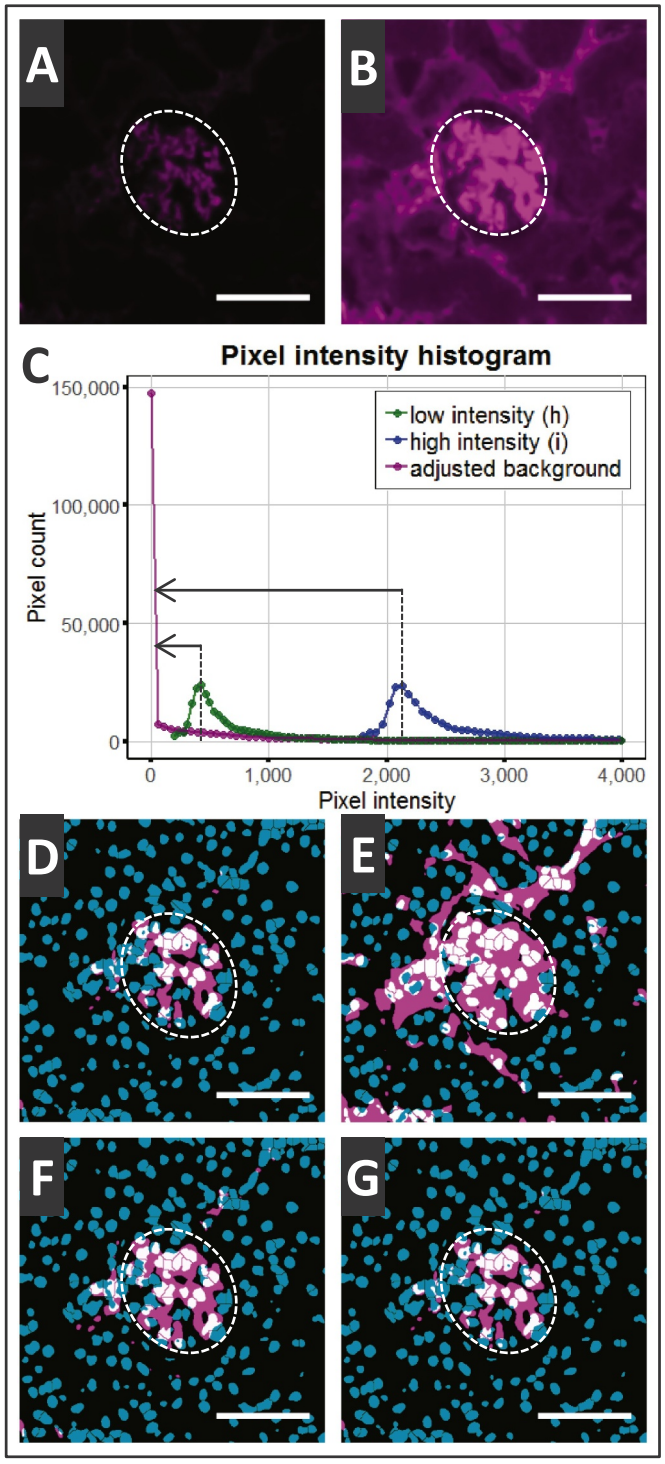

Fig. 3. Co-marker segmentation strategies.
α-8-integrin (magenta) staining of the detail from Fig. 1C with low (A, D, F) and high (B, E, G) signal and background intensity. Scale bar: 50 µm; glomerular area is indicated by white circle. **C,** Histogram analysis of pixel intensity: right-shift in pixel intensity in i (blue) compared to h (green). Linear shift of the histogram to set the maximum to zero (purple) equalizes the intensity distributions. Different thresholding methods for signal segmentation (D-G). A fixed threshold set to segment α-8-integrin positive signal in A (D) leads to wrong positive results when applied to B (E). A threshold adapted to median pixel intensity and intensity standard deviation delivers comparable results when applied to sections with differences in staining intensity (F-G). (For interpretation of the references to colour in this figure legend, the reader is referred to the web version of this article.)

in accumulation of extracellular matrix and hypertrophy. For more detailed conclusions on this model an evaluation of the staining with polarized light should be added to the analysis.

This example demonstrates the functionality and adaptability of the "AQUISTO" workflow to histochemical stainings.

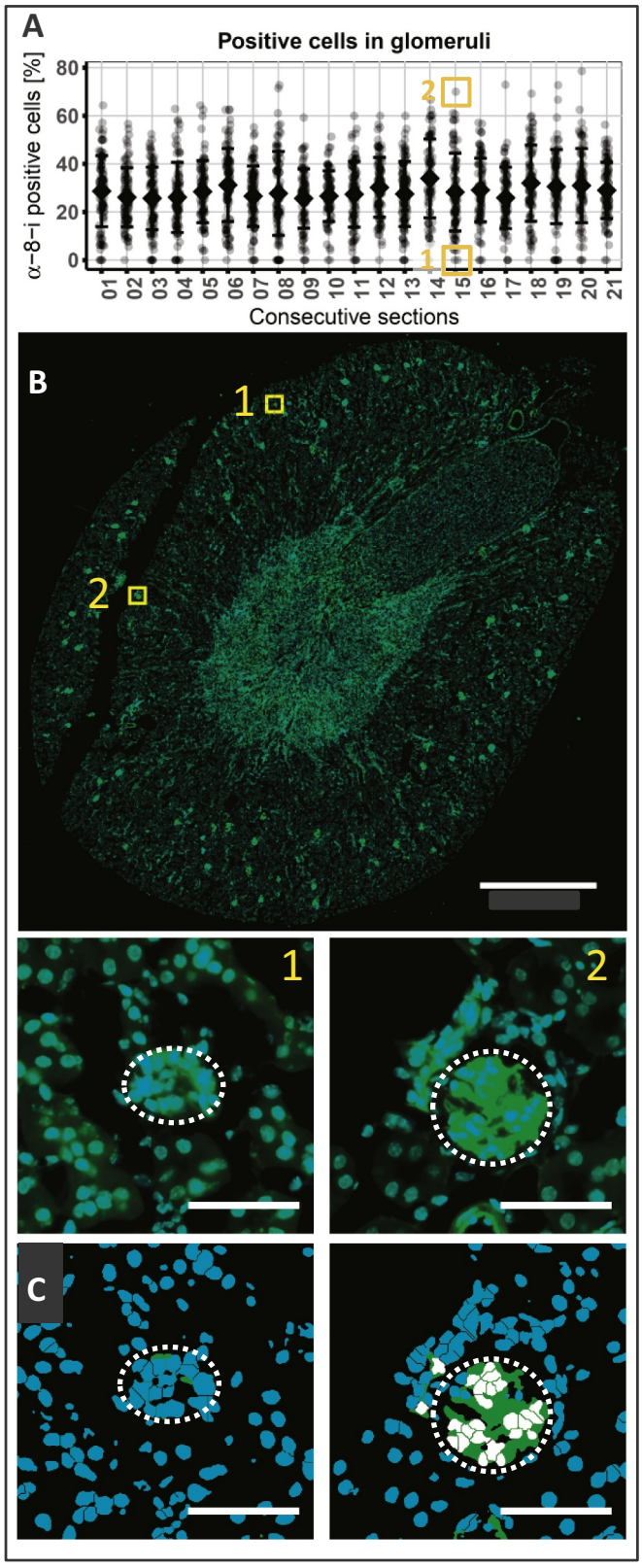

Fig. 4. Exemplaric quantification of cell counts in immunofluorescent sections, consistency in consecutive sections and backtracing of events.
A, Distribution of α-8-integrin positive cells in healthy mouse glomeruli evaluated by automatic detection after manual selection of glomeruli. Scatter dot plot of the fraction of α-8-integrin positive cells in each glomerulus with means and SD for 21 consecutive sections. Two glomeruli have been highlighted in the measured data (orange). **B,** Highlighted glomeruli (A) can be projected to the original image to visually verify the results (upper panel, highlight in yellow; scale bar: 1000 μm; staining: α-8-integrin – green and DAPI - cyan). Lower panels (Scale bar: 50 μm) are details indicated in (A). **C,** Segmentation of the details from b confirm the measured low percentage of α-8-integrin positive cells (white) in glomerulus 1 and the high percentage measured in glomerulus 2. (For interpretation of the references to colour in this figure legend, the reader is referred to the web version of this article.)

3.6. Verification of co-marker detection and representativeness of a single histological section

To verify the sensitivity of our analysis approach to rare events, we directly compared it with manual analysis of identical samples and FACS-analysis of tissue obtained from the same kidney. For this verification, we evaluated the number of renin positive cells. In the adult kidney, renin cells are located adjacent to the glomerulus in the wall of the afferent arteriole. Renin cells are the source of renin for the plasma renin-angiotensin system, the main regulator of blood pressure homeostasis [22]. Moreover, we and others recently identified the renin cells as a renewable progenitor cell niche important for kidney integrity in health and disease [6–8]. The low number of renin positive cells, which estimates to approximately 0.1% of renal cell mass [8], complicates assessment and exact quantification of renin expression. To test the sensitivity of our "AQUISTO" tool, we quantified renin expression in a recently described mouse model of renin deficiency [7]. Mice with an inducible renin cell-specific knockout of the stimulatory G protein α-subunit (henceforth "Gsα deficient mice") show a transiently reduced renin expression in immunofluorescent staining after pulse induction of recombination [7]. We used our novel approach to evaluate the decline of renin cell number in adult Gsα mice during continuous doxycyline induction of recombination in adult Gsα deficient mice, which constantly switches off its renin expression. By using a threshold adapted to the median pixel intensity and intensity standard deviation we could robustly detect remaining renin signal, despite the reduction of signal intensity in Gsα deficient mice (Fig. 6A).

Until now a manual semiquantitative assessment termed "renin index" [7] was utilized for histological quantification of renin producing cells, which binary classifies glomeruli by renin signal near the respective glomerulus. The renin index revealed a significant reduction of renin expression in Gsα deficient mice after one month of continuous induction, compared to the controls (Fig. 6B, upper panel, $p = .005$). However, three months after induction the renin index was not significantly different between control and Gsα deficient mice, possibly due to the high variance in this evaluation ($p = .080$). By automated analysis, we could observe a significant reduction of renin positive cells after one and three months of induction in Gsα deficient mice compared to their controls (Fig. 6B, middle panel, both timepoints $p < .001$). We could fully reproduce the results obtained by automatic immunostaining analysis with FACS (Fig. 6B, lower panel, $p = .026$ after 1 month, $p = .004$ after 3 months, Suppl. Fig. 3). Direct comparison of our new method and FACS revealed a strong direct correlation (slope: 1.09; $p = 2.5 \times 10^{-12}$ with Pearson's correlation coefficient; Fig. 6C). The R^2 value of 0.595 reflected the inherent variations of both methods. Thus, automatic "AQUISTO" quantification is comparable to classic FACS analysis and superior to manual scoring in determining the reduction of a rare cell population. These results also underline that the analysis of a single kidney section can reflect even small cellular subpopulations equally well as FACS analysis.

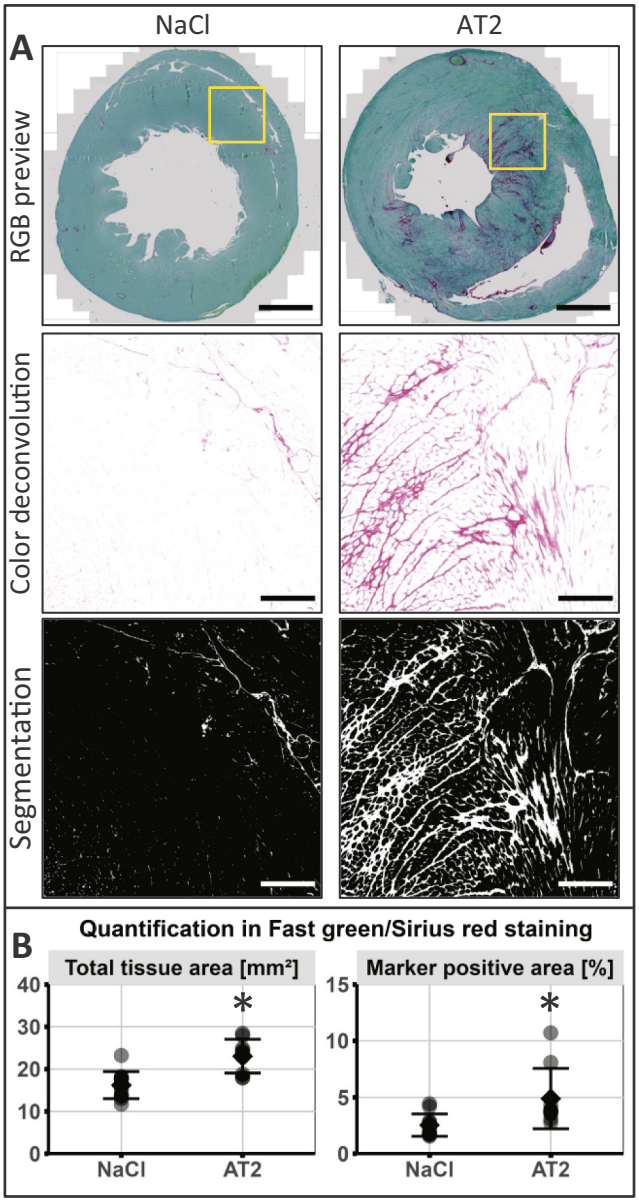

Fig. 5. Exemplaric quantification of tissue area in brightfield sections.
A, RGB-Previews of heart sections stained for collagen I and III (Fast green/Sirius red) after 4 week NaCl (control) or AT2 treatment with details (indicated by yellow rectangle) in heart sections from mice, scale bar: 1000 µm. Colour deconvolution with a giemsa vector leads to unmixing of the image, allowing for a segmentation of the marker-positive area to a binary image, scale bar: 200 µm. **B**, Measurement of total tissue area and fraction of marker positive area shows significant increase in AT2-treated animals compared to controls (*$p < .05$ NaCl vs AT2, *t*-test). (For interpretation of the references to colour in this figure legend, the reader is referred to the web version of this article.)

3.7. Quantification of cellular markers and morphological parameters

Another important question in any research field concerning injury and repair is the balance of cell proliferation and cell death. We used "AQUISTO" for quantitative evaluation of corresponding nuclear markers and morphometric parameters in whole kidney sections after injury with two different disease inducing sera. We chose proliferating cells nuclear antigen (PCNA) and terminal deoxynucleotidyl transferase-mediated dUTP-biotin nick end labeling (TUNEL) as markers for proliferation and cell death, respectively. For automatic quantification of both co-markers a semiautomatic selection of medulla, CTI and glomeruli was performed. To ensure a valid automatic detection of TUNEL signals, marker thresholds were adjusted to negative, without 5-ethynyl-2′-deoxyuridine-5′-triphosphate (EdUTP), and positive staining controls, after DNase digestion (Suppl. Fig. 7A, B). We were able to uniformly segment PCNA and TUNEL staining with a fixed threshold after background subtraction in all kidney compartments and automatically determine the percentage of positive cells for both markers in the kidney sections. While serum 1 showed a tendency towards high rates of cell death and low rates of proliferation in glomeruli, serum 2 had opposing effects (Fig. 7A, Suppl. Fig. 7C) with a significantly higher fraction of PCNA positive cells in the glomeruli at day 2 ($p = .037$). In medulla and CTI the PCNA positivity was significantly elevated with serum 2 at day 6 ($p = .012$ and $p = .007$, respectively).

To interpret this differential pattern of PCNA and TUNEL positivity in glomeruli in the context of tissue architecture we additionally analyzed glomerular morphological parameters. Serum 2 induced intraglomerular cell proliferation at day 2, resulting in significantly enlarged ($p = .018$ at day 2 and $p = .002$ at day 6) and nucleus-rich glomeruli ($p = .022$ at day 2, Fig. 7B).

3.8. Quantification of signaling pathways

To further expand the applicability of our approach, we quantified changes in the transforming growth factor β (TGF-β) signaling pathway in kidney tissue. TGF-β signaling is activated in diabetic nephropathy, mediating the development of long-term complications [23]. With a fixed threshold we quantified phosphorylated SMAD2/3 (p-SMAD2/3), a direct target of the TGF-β receptor tyrosine kinase [24], in kidney sections of animals with STZ induced diabetes and respective healthy controls. Staining of p-SMAD2/3 resulted in positive nuclear signal with a high heterogeneity in co-marker channel coverage of nuclei among the p-SMAD2/3 positive nuclei (Fig. 8A). We used a database query to determine the quota of p-SMAD2/3 signal coverage per DAPI positive area in all nuclei and analyzed their numerical distribution. We observed a tissue compartment-dependent difference of p-SMAD2/3 baseline abundance in healthy control animals (Fig. 8B). We could also detect a significant shift of p-SMAD2/3 coverage distribution in nuclei to a higher coverage in the medulla of diabetic animals compared to the healthy controls ($p < .001$), but not in glomeruli or CTI.

3.9. Simple adaptation of workflow demonstrates versatility

Finally, we modified our approach to detect and quantify DNA double strand breaks in the genome of mouse epidermal cells. DNA double strand breaks were induced using ionizing radiation and a genetic model that impairs DNA repair resulting in epidermal tumors [12]. Sections from irradiated, tumor and control skin were isolated and stained for nuclear phosphorylated histone 2AX (γH2AX), a marker for DNA double-strand breaks [25] (Fig. 9A-B). The γH2AX foci were localized by automatic maxima detection (Fig. 9C) and segmented epidermal nuclei were classified by their respective foci count in the database. The relative number of detected high foci-count nuclei was increased in tumor and irradiated skin compared to healthy control skin (Fig. 9D), reproducing results obtained by labour intensive manual quantification [12]. This example demonstrates the flexibility of our approach to adapt to a wide spectrum of staining analysis applications in the field of biomedical research.

4. Discussion

We described a workflow termed "AQUISTO", designed to automatically analyze large numbers of intact tissue sections on cellular scale, combining immunofluorescent or histochemical stainings with automated image data acquisition and quantification. Whole sections can be analyzed in an unbiased and reproducible fashion. "AQUISTO" comprises a tool that can efficiently evaluate different stainings in

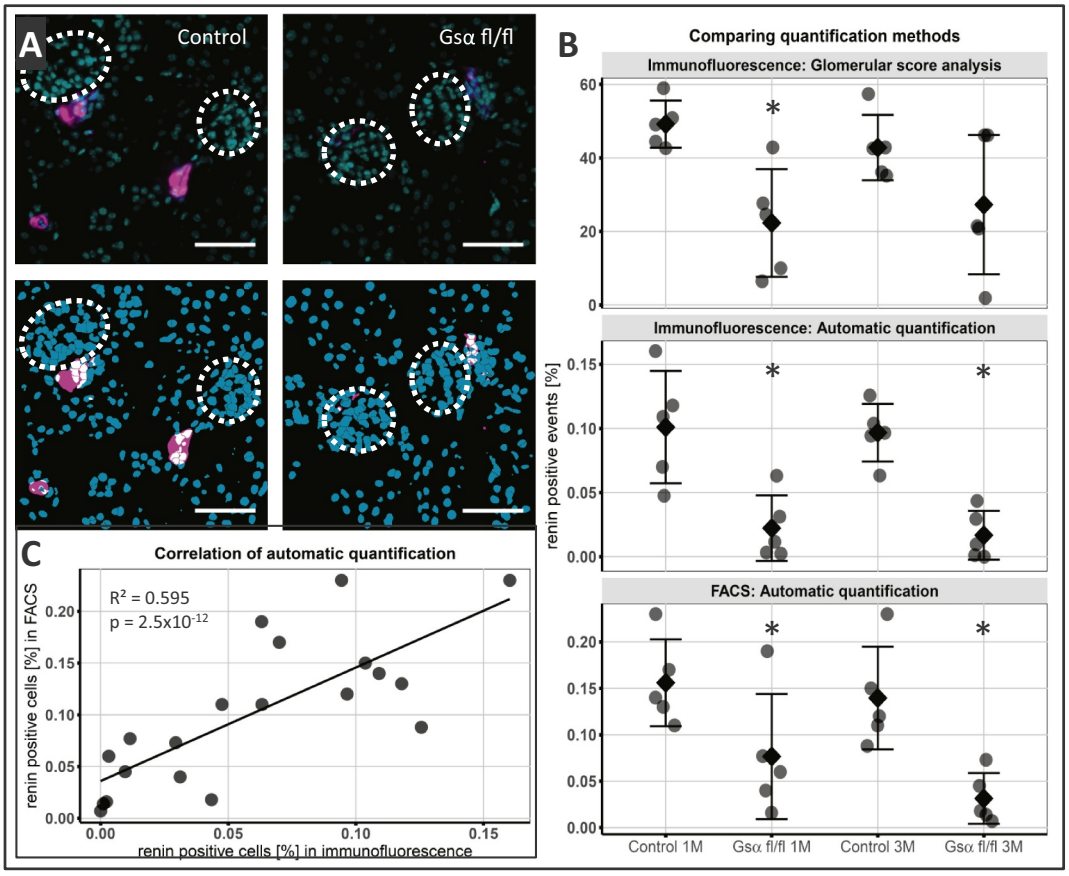

Fig. 6. Verification of co-marker detection.
A, Representative images of kidney cortex in Gsα deficient mice (right panels) and respective controls (left panels) after 3 months of continuous recombination induction by doxycycline. Sections were immunostained for renin (magenta) and DAPI (cyan). Upper panels show original image data, lower panels show segmented renin positive area (magenta), detected nuclei (cyan) and their overlap (renin positive nuclei, white). Scale bar: 50 µm; glomerular area is indicated by white circle. **B,** Renal renin cell content 1 month and 3 month after start of induction. Direct comparison of semiautomatic glomerular score analysis (upper panel, percentage of glomeruli with adjacent renin signal), automatic immunofluorescence approach (middle panel, percentage of renin positive cells in the section) and FACS analysis (lower panel, percentage of renin positive cells within gated cells). $n = 5$ animals per group, scatter dot plot with mean and SD, *$p < .05$ Control vs Gsα fl/fl, pairwise t-test. **C,** Correlation of kidney FACS analysis "AQUISTO" quantification for each kidney with Pearson's correlation coefficient. (For interpretation of the references to colour in this figure legend, the reader is referred to the web version of this article.)

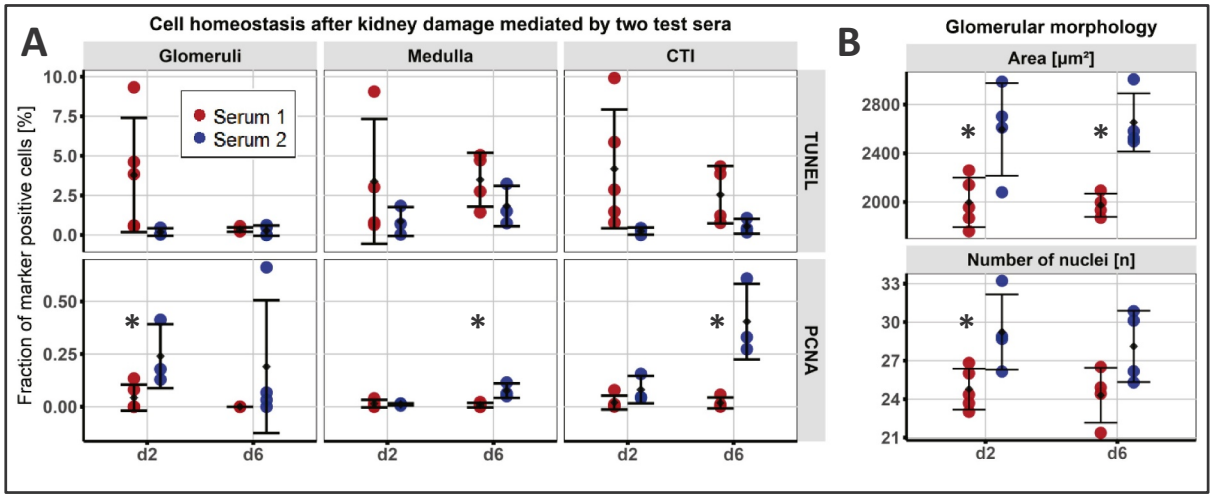

Fig. 7. Quantification of tissue homeostasis.
A, Relative number of TUNEL positive cells (upper panels) and PCNA positive cells (lower panels) in glomeruli, medulla and CTI of animals treated with two sera (serum 1: red, serum 2: blue). $n = 3–5$ animals per group, Scatter dot plot with means and SD, *$p < .05$ serum 1 vs. serum 2, pairwise t-test. **B,** Automatically determined glomerular morphology: mean glomerular area in sections (upper panel) and mean number of nuclei in glomeruli (lower panel). n = 3–5 animals per group, Scatter dot plot (serum 1: red, serum 2: blue) with means and SD, *$p < .05$ serum 1 vs. serum 2, pairwise t-test. (For interpretation of the references to colour in this figure legend, the reader is referred to the web version of this article.)

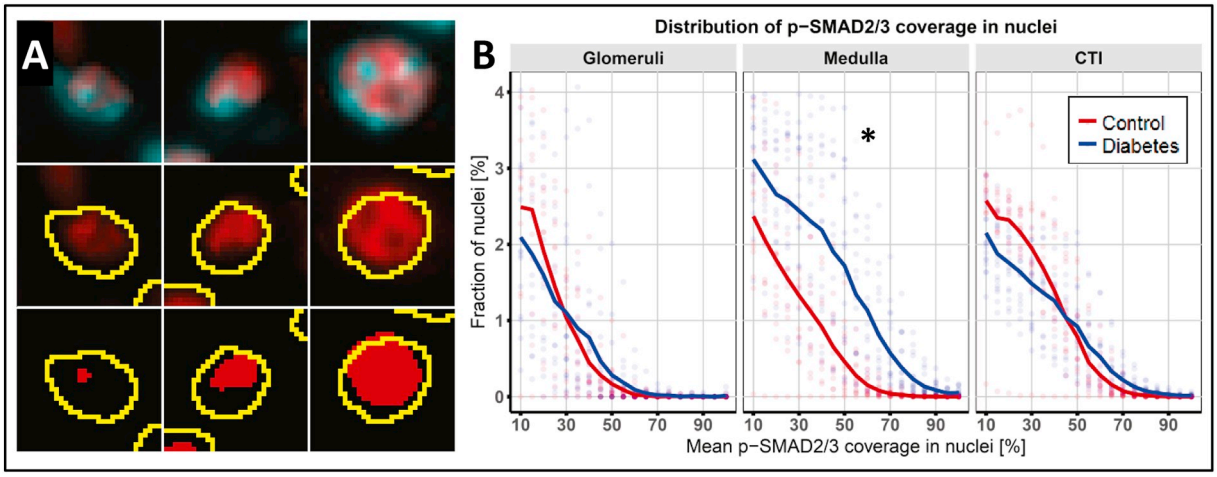

Fig. 8. Quantification of signaling pathway activation.
A, Heterogeneous p-SMAD2/3 coverage (red) in kidney nuclei (cyan). Low (left), mean (middle) and high (right) nuclear coverage in the original image (top), after automatic nucleus detection (center, nuclear boundaries in yellow) and after co-marker segmentation (bottom, p-SMAD2/3 positive area in red). **B**, Histograms of relative nuclear coverage by p-SMAD2/3 signal in glomeruli, medulla and CTI. Lines indicate mean values within the groups (healthy control: red, diabetic animals: blue). n = 14–18 animals per group, *p < .05 Control vs. Diabetes, pairwise t-test. (For interpretation of the references to colour in this figure legend, the reader is referred to the web version of this article.)

whole experimental sets in order to gain insight in (patho-) physiological processes relevant for biomedical research.

The stainings included in this proof-of-concept study demonstrate functionality of the workflow independent of marker-localization (nuclear, cytoplasmic, extracellular), type of staining (immunofluorescent or histochemical) and organ (kidney, heart, pancreas, skin). Additionally it can be easily validated and applied to the analysis of further samples (Suppl. Fig. 8). We validated nuclear detection for kidney sections and could assess up to 100,000 nuclei per section. The consistency of the results throughout consecutive kidney sections was proven in an example as well as the representativeness of a single section, even for the quantification of rare events. The accuracy of the acquired results was determined by direct comparison with a method of manual scoring and cell counts in FACS and showed superiority towards the manual approach and a significant correlation to FACS analysis. We established the possibility to combine the quantification of marker-positive cells with morphometric parameters, like tissue area and cellular density, for the detection of hypertrophy or hyperplasia. With the help of histogram distribution analysis for the gradual assessment of nuclear marker coverage the approach can reliably detect changes in signaling pathway activation. Especially in structurally complex organs like the kidney, with functionally distinct tissue compartments, the need for differentiated analysis of tissue areas becomes evident in the examples included in this manuscript. The quantification of DNA double strand breaks in the genome of mouse epidermal cells is only one example about how the workflow could easily be adapted to answer further biologically relevant questions. Instead of measuring marker coverage in the nuclei, the number of maxima in the marker channel is analyzed, demonstrating the general flexibility of our approach.

Although the list of applications might appear out of context, it can create an impression about the inherent possibilities of “AQUISTO” when applied to the analysis of whole experimental sets. Consider the characterization of interactions of different cell types and extracellular matrix in any disease model. With “AQUISTO” it would be possible to automatically analyze tissue sections for many different aspects of cellular signaling and function. Next to the histochemical of staining extracellular matrix, it is possible to identify cell types associated with the production of these proteins. At the same time, structural changes in cell number or tissue area can be detected and brought into context with stainings for cell death, senescence and proliferation. Disease progression and chronification is often an effect of inflammation, so the quantification of different types of cytokines and immune cells could be beneficial to understand the pathogenesis. Additionally, it is possible to analyze changes in signaling pathway activation, which might contribute to abnormal cellular behavior and translational programs. All these possibilities can then be focused on certain tissue compartments, to understand local mechanisms or the contribution of certain environmental niches in complex organs.

Apart from the clear advantages, we could also identify limitations of the approach which however are common to all histological methods (Suppl. Fig. 9). The analysis has only limited robustness towards poor sample preparation and image acquisition. Another bottleneck in the entire workflow is the reliability and quality of antibody-detection, which has to be carefully validated for tissue type and staining protocol, as recently performed for extracellular matrix [26]. Our method can compete with FACS analysis in cell count number, but it is more restricted in the number of multiplexed markers and the analysis of membrane stainings. A major field of application for flow cytometry is the characterization of inflammatory responses. Although it is generally possible to analyze markers of inflammation with “AQUISTO” the feasibility is restricted by the general limitations of histological stainings, like staining quality and marker multiplexing. Additionally some immune cells have segmented nuclei and require further adaptation and evaluation of the necessary parameters for nucleus detection. In general, we also strongly recommend processing coherent experimental sets in parallel, including appropriate controls (samples from healthy or sham-treated animals as well as staining controls) as reference for data interpretation and normalization. The necessity of these controls and visual verification steps is underlined by the fact that our approach relies on one major input: Processing and segmentation parameters are set by visual justification in a subset of samples for every staining set. This allows for a certain variability of the numerical results that might lead to controversial discussions about objectivity and reliability of the method. However this would also apply to setting gating strategies for FACS or manual counting, only that human perception of signal intensities is not linear or fixed [27] and thus manual counting would be more prone to bias and variability. By utilizing the same processing parameters to every sample in a staining set, the differences are of systematic nature.

Automatic processing of image files has become increasingly popular, with a high number of very specialized software tools [2] and approaches for image analysis [28]. Our approach, although developed

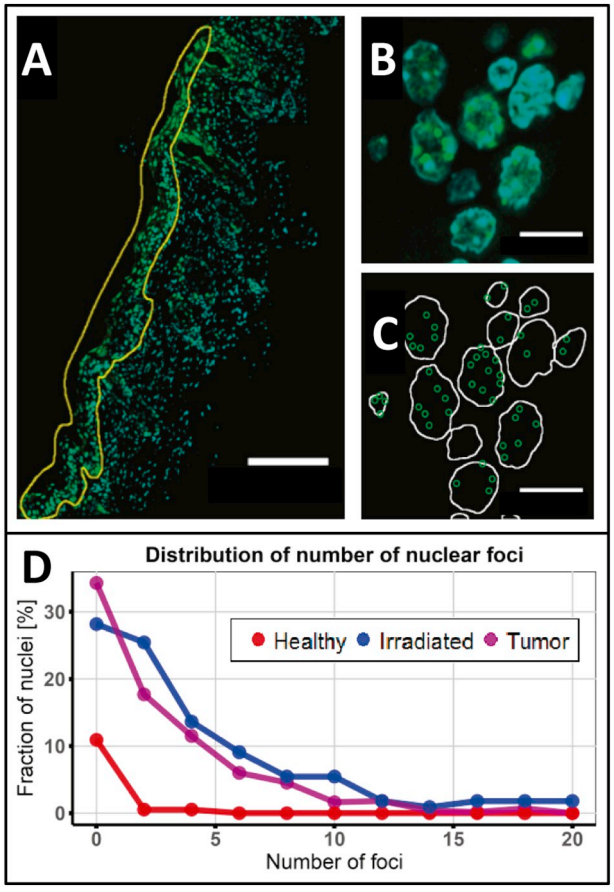

Fig. 9. Adaptability of the workflow.
A-D, gH2AX staining (green) in mouse epidermal skin tumor, nuclei stained with DAPI (cyan). Yellow outline indicates manually selected area of skin tumor (A; scale bar: 200 µm). **B–C**, Magnification from (A), illustrating focal staining of gH2AX (green) in nuclei (DAPI, cyan) and foci analysis with green circles representing automatically detected gH2AX foci (C). Scale bars: 10 µm. D, Histogram showing the number of repair foci per nucleus in healthy (red), irradiated (blue) and tumor skin (purple) for one section in each group. (For interpretation of the references to colour in this figure legend, the reader is referred to the web version of this article.)

mainly for kidney section analysis, comprises a very flexible and universal tool for the unbiased analysis of histologically stained tissue images. The principle of automatic counting has been widely adapted in high-throughput imaging of cell cultures [1,29] and there are publications about the analysis of cellular subpopulations in whole histological tissue sections [30]. However these are often only applied to very specific scientific questions and sets of markers. Our approach combines a complete computer assisted workflow, including database management, image preparation, parameter setting, image processing and data analysis, starting with the microscopy images up until the creation of first graphs for different experimental groups. It is incorporated in a step by step graphic user interface. While it is linear enough to be time-saving and user-friendly, it remains versatile enough to be validated and applied to the analysis of different organs, staining techniques and markers without expert programming skills. The structure of each dataset allows absolute reproducibility with the option of easy manual re-evaluation of each entity. The number of multiplexed markers is theoretically only limited by the type of staining and the capabilities of the microscope to recognize different emission spectra. Although companies specialized on microscopy also offer image analysis solutions and there are commercially available options as well, the establishment of an open source workflow provides multiple advantages: Additional to the financial aspects, FIJI and R are well established software platforms with a diverse community of users, covering various fields of expertise, from general statistics, over informatics to biology. This community could naturally contribute to the further development of the basic workflow presented in this study, depending on demand and not necessarily on financial interest. It is easy to implement additional image processing and measurements to further modify the resulting database, and make full use of the existing processing approaches. For example there are already different methods for colour deconvolution provided by a FIJI-plugin, which enable the unmixing and subsequent segmentation of various types of histochemical stainings (e.g. PAS, Giemsa, Masson-Goldner-Trichrome). Due to the acquisition of multiple parameters for every single nucleus the database can be queried in a multitude of ways to answer more complex questions.

Therefore, the “AQUISTO” workflow could transfer multiple positive aspects of automatic quantification to organ level, most importantly the elimination of individual bias from analysis. Taken together with the high number of cells included in the analysis, which cannot be counted manually in reasonable time spans, the approach can be most objective. Deviations in classification of nuclei or co-marker positivity are of systematic nature and their impact could be minimized when comparing experimental groups and their respective controls. This facilitates sophisticated analyses as well as screening approaches for rare phenomena in complex organs.

5. Conclusion

In the present study, we describe the basic principle and application of an approach to automatic whole section analysis, termed “AQUISTO”. Potential applications extend far beyond the herein provided examples - we see a general applicability as a basic workflow in biological research. Taken together, our automatic image analysis approach is able to combine advantages of the high cells counts of flow cytometry and the maintenance of tissue integrity in histology, helping to overcome typical methodic restrictions. It is a user-friendly, versatile and easily implementable tool for large-scale quantification of tissue sections, with various possibilities for further development.

Acknowledgements

The authors gratefully thank Silke Tulok, Ellen Geibelt, Anika Lüdemann and Katharina Hüttner for their technical assistance. This work was supported by the Light Microscopy Facility, a Core Facility of the CMCB Technology Platform at Technische Universität Dresden and the CFCI (Core Facility Cellular Imaging) at the Carl Gustav Carus Faculty of Medicine. F.G. is funded by a grant from the DFG (GE 2845/1-1). This work was supported by DFG (TO 679/2-1, TO 679/3-1, HU 600/6-1, HU 600/8-1). We also thank Prof. Andreas Deussen for his thorough evaluation and comments on the final manuscript. We are very much indebted to Lee S. Weinstein, Min Chen and Jürgen Schnermann from NIH-NIDDK for providing transgenic mice.

Author contributions

Friederike Kessel: Conceptualization, Methodology, Software, Validation, Formal Analysis, Investigation, Data Curation, Writing – Original Draft, Review & Editing, Visualization. **Anne Steglich:** Conceptualization, Validation, Investigation, Data Curation, Writing – Review & Editing. **Todor Tschongov:** Conceptualization, Investigation. **Florian Gembardt:** Investigation, Writing – Review & Editing, Funding Acquisition. **Leo Ruhnke:** Investigation. **Julian Stumpf:** Investigation. **Rayk Behrendt:** Investigation, Resources. **Christian Cohrs:** Investigation, Resources. **Irakli Kopaliani:** Investigation, Resources. **Vladimir Todorov:** Conceptualization, Writing – Review & Editing, Funding Acquisition. **Michael Gerlach:** Conceptualization, Methodology, Software, Validation, Writing – Original Draft, Review &

Editing. **Christian Hugo:** Conceptualization, Writing – Review & Editing, Funding Acquisition.

Declarations of competing interests

None.

Appendix A. Supplementary data

Supplementary data to this article can be found online at https://doi.org/10.1016/j.cellsig.2019.05.020.

References

[1] S. van Teeffelen, J.W. Shaevitz, Z. Gitai, Image analysis in fluorescence microscopy: bacterial dynamics as a case study, Bioessays 34 (5) (2012) 427–436.

[2] K.W. Eliceiri, M.R. Berthold, I.G. Goldberg, L. Ibanez, B.S. Manjunath, M.E. Martone, R.F. Murphy, H. Peng, A.L. Plant, B. Roysam, N. Stuurman, J.R. Swedlow, P. Tomancak, A.E. Carpenter, Biological imaging software tools, Nat. Methods 9 (7) (2012) 697–710.

[3] J. Schindelin, I. Arganda-Carreras, E. Frise, V. Kaynig, M. Longair, T. Pietzsch, S. Preibisch, C. Rueden, S. Saalfeld, B. Schmid, J.Y. Tinevez, D.J. White, V. Hartenstein, K. Eliceiri, P. Tomancak, A. Cardona, Fiji: an open-source platform for biological-image analysis, Nat. Methods 9 (7) (2012) 676–682.

[4] S. N, V. S, Image segmentation by using thresholding techniques for medical images, Comput. Sci. Eng. 6 (1) (2016) 1–13.

[5] R Development Core Team, R: A Language and Environment for Statistical Computing, R Foundation for Statistical Computing, (2008).

[6] C. Starke, H. Betz, L. Hickmann, P. Lachmann, B. Neubauer, J.B. Kopp, M.L. Sequeira-Lopez, R.A. Gomez, B. Hohenstein, V.T. Todorov, C.P. Hugo, Renin lineage cells repopulate the glomerular mesangium after injury, J. Am. Soc. Nephrol. 26 (1) (2015) 48–54.

[7] P. Lachmann, L. Hickmann, A. Steglich, M. Al-Mekhlafi, M. Gerlach, N. Jetschin, S. Jahn, B. Hamann, M. Wnuk, K. Madsen, V. Djonov, M. Chen, L.S. Weinstein, B. Hohenstein, C.P.M. Hugo, V.T. Todorov, Interference with Gsalpha-coupled receptor signaling in renin-producing cells leads to renal endothelial damage, J. Am. Soc. Nephrol. 28 (12) (2017) 3479–3489.

[8] L. Hickmann, A. Steglich, M. Gerlach, M. Al-Mekhlafi, J. Sradnick, P. Lachmann, M.L.S. Sequeira-Lopez, R.A. Gomez, B. Hohenstein, C. Hugo, V.T. Todorov, Persistent and inducible neogenesis repopulates progenitor renin lineage cells in the kidney, Kidney Int. 92 (6) (2017) 1419–1432.

[9] J. Sradnick, S. Rong, A. Luedemann, S.P. Parmentier, C. Bartaun, V.T. Todorov, F. Gueler, C.P. Hugo, B. Hohenstein, Extrarenal progenitor cells do not contribute to renal endothelial repair, J. Am. Soc. Nephrol. 27 (6) (2016) 1714–1726.

[10] S. Al-Gburi, A.J. Deussen, R. Galli, M.H. Muders, B. Zatschler, A. Neisser, B. Muller, I. Kopaliani, Sex-specific differences in age-dependent progression of aortic dysfunction and related cardiac remodeling in spontaneously hypertensive rats, Am. J. Phys. Regul. Integr. Comp. Phys. 312 (5) (2017) R835–R849.

[11] H. Chmelova, C.M. Cohrs, J.A. Chouinard, C. Petzold, M. Kuhn, C. Chen, I. Roeder, K. Kretschmer, S. Speier, Distinct roles of beta-cell mass and function during type 1 diabetes onset and remission, Diabetes 64 (6) (2015) 2148–2160.

[12] B. Hiller, A. Hoppe, C. Haase, C. Hiller, N. Schubert, W. Muller, M.A.M. Reijns, A.P. Jackson, T.A. Kunkel, J. Wenzel, R. Behrendt, A. Roers, Ribonucleotide excision repair is essential to prevent squamous cell carcinoma of the skin, Cancer Res. 20 (2018) 5917–5926.

[13] RStudio Team, RStudio: Integrated Development Environment for R, RStudio Inc, Boston, MA, 2016.

[14] H. Wickham, ggplot2: Elegant Graphics for Data Analysis, Springer-Verlag, New York, 2009.

[15] H. Wickham, Reshaping data with the {reshape} package, J. Stat. Softw. 21 (2007) 1–20.

[16] D. Legland, I. Arganda-Carreras, P. Andrey, MorphoLibJ: integrated library and plugins for mathematical morphology with ImageJ, Bioinformatics 32 (22) (2016) 3532–3534.

[17] J.D. Ruifrok AC1, Quantification of Histochemical Staining by Color Deconvolution, vol. 23, (2001), pp. 291–299.

[18] Sternberg, Biomed. Image Process. 16 (1) (1983) 22–34 Computer.

[19] Y.M. Scindia, U.S. Deshmukh, H. Bagavant, Mesangial pathology in glomerular disease: targets for therapeutic intervention, Adv. Drug Deliv. Rev. 62 (14) (2010) 1337–1343.

[20] S.D. Wicksell, The corpuscle problem. A mathematical study of a biometric problem, Biometrika 17 (1–2) (1925) 84–99.

[21] P. Brecher, Angiotensin II and cardiac fibrosis, Trends Cardiovascular Med. 6 (6) (1996) 193–198.

[22] H. Castrop, K. Hocherl, A. Kurtz, F. Schweda, V. Todorov, C. Wagner, Physiology of kidney renin, Physiol. Rev. 90 (2) (2010) 607–673.

[23] F.N. Ziyadeh, Mediators of diabetic renal disease: the case for TGF-beta as the major mediator, J. Am. Soc. Nephrol. 15 (1) (2004) S55–S57.

[24] M.-S.M. Abdollah S1, T. Tsukazaki, H. Hayashi, L. Attisano, J.L. Wrana, TbetaRI phosphorylation of Smad2 on Ser465 and Ser467 is required for Smad2-Smad4 complex formation and signaling, JBC 272 (1997) 2768–27685.

[25] E.P. Rogakou, D.R. Pilch, A.H. Orr, V.S. Ivanova, W.M. Bonner, DNA double-stranded breaks induce histone H2AX phosphorylation on serine 139, J. Biol. Chem. 273 (10) (1998) 5858–5868.

[26] S. Rickelt, R.O. Hynes, Antibodies and methods for immunohistochemistry of extracellular matrix proteins, Matrix Biol. 71-72 (2018) 10–27.

[27] H.B. Barlow, Temporal and spatial summation in human vision at different background intensities, J. Physiol.-Lond. 141 (2) (1958) 337–350.

[28] M.N. Gurcan, L.E. Boucheron, A. Can, A. Madabhushi, N.M. Rajpoot, B. Yener, Histopathological image analysis: a review, IEEE Rev. Biomed. Eng. 2 (2009) 147–171.

[29] D. Bertin, N. Jourde-Chiche, P. Bongrand, N. Bardin, Original approach for automated quantification of antinuclear autoantibodies by indirect immunofluorescence, Clin. Dev. Immunol. 2013 (2013) 182172.

[30] S. Blom, L. Paavolainen, D. Bychkov, R. Turkki, P. Maki-Teeri, A. Hemmes, K. Valimaki, J. Lundin, O. Kallioniemi, T. Pellinen, Systems pathology by multiplexed immunohistochemistry and whole-slide digital image analysis, Sci. Rep. 7 (1) (2017) 15580.